

**Dipolar-octupolar Ising antiferromagnetism in  $\text{Sm}_2\text{Ti}_2\text{O}_7$ : A moment fragmentation candidate**

C. Mauws,<sup>1,2</sup> A. M. Hallas,<sup>3,4</sup> G. Sala,<sup>5</sup> A. A. Aczel,<sup>5</sup> P. M. Sarte,<sup>6,7</sup> J. Gaudet,<sup>3</sup> D. Ziat,<sup>8</sup> J. A. Quilliam,<sup>8</sup> J. A. Lussier,<sup>1</sup> M. Bieringer,<sup>1</sup> H. D. Zhou,<sup>9,10</sup> A. Wildes,<sup>11</sup> M. B. Stone,<sup>5</sup> D. Abernathy,<sup>5</sup> G. M. Luke,<sup>3,12,13</sup> B. D. Gaulin,<sup>3,12</sup> and C. R. Wiebe<sup>1,2,3,12</sup>

<sup>1</sup>*Department of Chemistry, University of Manitoba, Winnipeg, Manitoba, Canada R3T 2N2*

<sup>2</sup>*Department of Chemistry, University of Winnipeg, Winnipeg, Manitoba, Canada R3B 2E9*

<sup>3</sup>*Department of Physics and Astronomy, McMaster University, Hamilton, Ontario, Canada L8S 4M1*

<sup>4</sup>*Department of Physics and Astronomy and Rice Center for Quantum Materials, Rice University, Houston, Texas 77005, USA*

<sup>5</sup>*Neutron Scattering Division, Oak Ridge National Laboratory, Oak Ridge, Tennessee 37831, USA*

<sup>6</sup>*School of Chemistry, University of Edinburgh, Edinburgh EH9 3FJ, United Kingdom*

<sup>7</sup>*Centre for Science at Extreme Conditions, University of Edinburgh, Edinburgh EH9 3FD, United Kingdom*

<sup>8</sup>*Institut Quantique and Département de Physique, Université de Sherbrooke, Sherbrooke, Québec, Canada J1K 2R1*

<sup>9</sup>*Department of Physics and Astronomy, University of Tennessee-Knoxville, Knoxville, Tennessee 37996-1220, USA*

<sup>10</sup>*National High Magnetic Field Laboratory, Florida State University, Tallahassee, Florida 32306-4005, USA*

<sup>11</sup>*Institut Laue-Langevin, 71 avenue des Martyrs, CS 20156, 38042 Grenoble Cedex 9, France*

<sup>12</sup>*Canadian Institute for Advanced Research, Toronto, Ontario, Canada M5G 1M1*

<sup>13</sup>*TRIUMF, 4004 Wesbrook Mall, Vancouver, British Columbia, Canada V6T 2A3*



(Received 11 May 2018; published 5 September 2018)

Over the past two decades, the magnetic ground states of all rare-earth titanate pyrochlores have been extensively studied, with the exception of  $\text{Sm}_2\text{Ti}_2\text{O}_7$ . This is, in large part, due to the very high absorption cross section of naturally occurring samarium, which renders neutron scattering infeasible. To combat this, we have grown a large, isotopically enriched single crystal of  $\text{Sm}_2\text{Ti}_2\text{O}_7$ . Using inelastic neutron scattering, we determine that the crystal field ground state for  $\text{Sm}^{3+}$  is a dipolar-octupolar doublet with Ising anisotropy. Neutron diffraction experiments reveal that  $\text{Sm}_2\text{Ti}_2\text{O}_7$  orders into the all-in, all-out magnetic structure with an ordered moment of  $0.44(7)\mu_B$  below  $T_N = 0.35$  K, consistent with expectations for antiferromagnetically coupled Ising spins on the pyrochlore lattice. Zero-field muon spin relaxation measurements reveal an absence of spontaneous oscillations and persistent spin fluctuations down to 0.03 K. The combination of the dipolar-octupolar nature of the  $\text{Sm}^{3+}$  moment, the all-in, all-out ordered state, and the low-temperature persistent spin dynamics make this material an intriguing candidate for moment fragmentation physics.

DOI: [10.1103/PhysRevB.98.100401](https://doi.org/10.1103/PhysRevB.98.100401)

Rare-earth titanate pyrochlores of the form  $R_2\text{Ti}_2\text{O}_7$  have long been a centerpiece in the study of geometrically frustrated magnetism [1]. In this family of materials, the magnetism is carried by the  $R^{3+}$  rare-earth ions, which decorate a network of corner-sharing tetrahedra. The study of this family has led to the discovery of a range of fascinating ground states such as the dipolar spin ice state, which was first observed in  $\text{Ho}_2\text{Ti}_2\text{O}_7$  and  $\text{Dy}_2\text{Ti}_2\text{O}_7$  [2–4]. Here, local Ising anisotropy combines with dominant dipolar interactions, which are ferromagnetic at the nearest-neighbor level on the pyrochlore lattice [5]. The spin ice state is characterized by individual tetrahedra obeying two-in, two-out “ice rules,” wherein two spins point directly towards the tetrahedron’s center and the other two spins point outwards (left inset of Fig. 1). This configuration can be achieved in six equivalent ways for a single tetrahedron, giving rise to a macroscopic degeneracy for the lattice as a whole. In other titanates, where the rare-earth moments are smaller than in  $\text{Ho}_2\text{Ti}_2\text{O}_7$  and  $\text{Dy}_2\text{Ti}_2\text{O}_7$ , dipolar interactions become less important and exchange interactions tend to dominate. This is exactly the case when  $R = \text{Sm}^{3+}$  ( $\sim 1\mu_B$ ), where the magnetic moment is reduced by a factor of ten from  $R = \text{Ho}^{3+}$  and  $\text{Dy}^{3+}$  ( $\sim 10\mu_B$ ), corresponding

to dipolar interactions that are weaker by two orders of magnitude.

In this Rapid Communication, we show that antiferromagnetically coupled Ising spins with negligible dipolar interactions give rise to an all-in, all-out (AIAO) magnetic ground state in  $\text{Sm}_2\text{Ti}_2\text{O}_7$ . The AIAO structure is characterized by adjacent tetrahedra alternating between all spins pointing inwards and all spins pointing outwards (right inset of Fig. 1). Unlike the ferromagnetic spin ice state, the antiferromagnetic AIAO state does not give rise to a macroscopic degeneracy; placing a single spin as “in” or “out” is enough to uniquely constrain the orientations of all other spins on the lattice. A host of neodymium pyrochlores with varying nonmagnetic  $B$  sites also display the AIAO ground state,  $\text{Nd}_2\text{B}_2\text{O}_7$  ( $B = \text{Sn, Zr, Hf}$ ) [6–9].  $\text{Nd}_2\text{Zr}_2\text{O}_7$  is a particularly interesting case as magnetic Bragg peaks from the AIAO structure and disordered, spin-ice-like diffuse scattering coexist at low temperatures [10]. This exotic phenomenology has been termed moment fragmentation [11]. Recent theoretical work [12] has argued that the origin of this effect is the peculiar dipolar-octupolar symmetry of the  $\text{Nd}^{3+}$  ground-state doublet [7,8]. When combined with an AIAO ground state, the symmetry

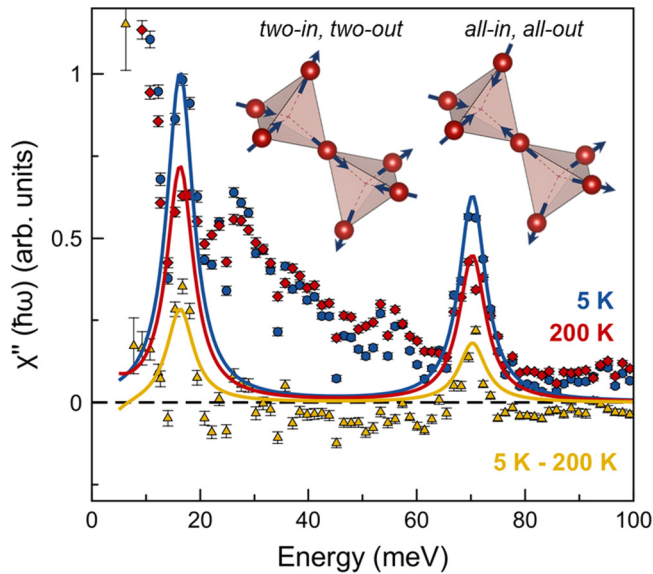


FIG. 1. Inelastic neutron scattering measurements of the crystal electric field (CEF) excitations in  $\text{Sm}_2\text{Ti}_2\text{O}_7$  at 5 K (blue) and 200 K (red). The temperature difference (yellow) confirms the presence of two CEF levels, at 16.3(5) meV and 70.0(5) meV. The fits to the data with our CEF model are given by the solid lines and reveal the Ising nature of the  $\text{Sm}^{3+}$  moments in  $\text{Sm}_2\text{Ti}_2\text{O}_7$ . The insets show the ferromagnetic Ising spin configuration (two-in, two-out) and the antiferromagnetic Ising spin configuration (all-in, all-out).

properties of this dipolar-octupolar doublet allow the decoupling of the divergence-full (AIAO) and divergence-free (spin ice) fluctuations [12]. Here, we use neutron spectroscopy to determine the dipolar-octupolar nature of the crystal field ground-state doublet of  $\text{Sm}_2\text{Ti}_2\text{O}_7$  and use neutron diffraction to show that it orders into an AIAO structure below  $T_N = 0.35$  K. Muon spin relaxation measurements reveal persistent spin dynamics within the magnetically ordered state, down to 0.03 K. Thus, we demonstrate that  $\text{Sm}_2\text{Ti}_2\text{O}_7$  possesses the requisite ingredients for moment fragmentation physics.

In contrast to the extensive studies that have been performed on the other magnetic titanate pyrochlores,  $R_2\text{Ti}_2\text{O}_7$  ( $R = \text{Gd}, \text{Tb}, \text{Dy}, \text{Ho}, \text{Er}, \text{Yb}$ ), the magnetic properties of  $\text{Sm}_2\text{Ti}_2\text{O}_7$  have remained largely unexplored. Prior studies of  $\text{Sm}_2\text{Ti}_2\text{O}_7$  were limited to bulk property measurements in the paramagnetic regime, above 0.5 K, which revealed weak antiferromagnetic interactions ( $\theta_{\text{CW}} = -0.26$  K) [13]. While the other above-mentioned titanate pyrochlores have been the subjects of a plethora of elastic and inelastic neutron scattering experiments, equivalent experiments on  $\text{Sm}_2\text{Ti}_2\text{O}_7$  are daunting. The first reason is the size of the  $\text{Sm}^{3+}$  magnetic moment; the Lande  $g$ -factor associated with the  $4f^5$  electronic configuration is its smallest possible nonzero value ( $g_J = \frac{2}{7}$ ), giving rise to small moments even in the absence of crystal field effects (which make the moment smaller still). This small magnetic moment represents a significant hindrance because scattered neutron intensity varies as the moment squared. Compounding this effect is that naturally occurring samarium is a very strong neutron absorber due to the presence of  $^{149}\text{Sm}$  at the 13.9% level ( $\sigma_{\text{abs}} = 42\,000$  b). Neutron scattering measurements of the type we report here

are only possible with a sample isotopically enriched with  $^{154}\text{Sm}$  ( $\sigma_{\text{abs}} = 8.4$  b). However, the neutron absorption cross section of  $^{149}\text{Sm}$  is so high that even trace amounts result in a sample that is still strongly absorbing by neutron scattering standards.

We grew a large single crystal of  $\text{Sm}_2\text{Ti}_2\text{O}_7$  with the optical floating zone technique using 99.8% enriched  $^{154}\text{Sm}_2\text{O}_3$  (Cambridge Isotopes). Low-temperature heat capacity measurements were performed using the quasiadiabatic technique. Neutron diffraction measurements were performed on the D7 polarized diffuse scattering spectrometer at the Institute Laue-Langevin and beam line HB-1A at the High Flux Isotope Reactor at Oak Ridge National Laboratory (ORNL). Inelastic neutron scattering measurements were performed on the ARCS [14] and SEQUOIA [15] spectrometers at the Spallation Neutron Source at ORNL. Muon spin relaxation measurements were carried out at TRIUMF. Further experimental details are provided in the Supplemental Material [16].

The Hund's rules ground state for  $\text{Sm}^{3+}$  is  $J = \frac{5}{2}$ . Accordingly, in the reduced symmetry environment of the pyrochlore lattice, the  $2J + 1 = 6$  states split into three Kramers' doublets, one of which forms the crystal electric field (CEF) ground state. Inelastic neutron scattering (INS) measurements on  $\text{Sm}_2\text{Ti}_2\text{O}_7$ , which are presented in Fig. 1 and Fig. S2, show intense excitations at 16.3(5) and 70.0(5) meV corresponding to transitions to the excited CEF doublets. The lower-energy excitation is consistent with one of the modes previously identified in Raman scattering experiments by Singh *et al.* [13]. However, other modes observed in Raman scattering and originally attributed to additional CEF excitations are not visible in our INS data. Malkin *et al.* attempted to determine the crystal field parameters of  $\text{Sm}_2\text{Ti}_2\text{O}_7$  by modeling magnetic susceptibility data [17]. This work predicts CEF levels at 21.4 and 26.4 meV, both of which are inconsistent with our INS data. It is worth noting that  $\text{Sm}^{3+}$  has a rather atypical form factor, which rather than monotonically decreasing with  $Q$  instead reaches its maximum value near  $5 \text{ \AA}^{-1}$ . Both of the CEF transitions observed here obey this form factor (see Supplemental Material [16]). These two excited states account for the full manifold associated with the  $J = \frac{5}{2}$  ground-state multiplet.

Next, we modeled the INS data in order to extract the crystal field Hamiltonian. This analysis is complicated by the strong residual absorption of  $^{149}\text{Sm}$  in the isotopically enriched single crystal. This issue was addressed by performing an absorption correction with Monte Carlo ray tracing simulations using MCVINE [18]. In the case of  $\text{Sm}^{3+}$ , the Hund's rules  $J$  manifold is separated from the first excited spin-orbit manifold by  $\lambda(J + 1) \approx 500$  meV [19]. Incorporating this higher manifold into our analysis would require the introduction of four additional free parameters. This would result in an underconstrained parametrization of the CEF Hamiltonian and thus we have neglected it here. Further details of these calculations and the subsequent determination of the CEF eigenvalues and eigenvectors are presented in the Supplemental Material [16].

The CEF parameters that provide the best fit to our INS data for  $\text{Sm}_2\text{Ti}_2\text{O}_7$  within a point charge approximation are  $B_{20} = 3.397$  meV,  $B_{40} = 0.123$  meV, and  $B_{43} = 8.28 \times 10^{-8}$  meV. Table I shows the resulting CEF eigenvectors and

TABLE I. Result of the CEF analysis for  $\text{Sm}_2\text{Ti}_2\text{O}_7$ , calculated within a point charge model and then refined by fitting the two experimentally observed CEF excitations.

$E_{\text{obs}}$ (meV)	$E_{\text{fit}}$ (meV)	$ \pm\frac{5}{2}\rangle$	$ \pm\frac{3}{2}\rangle$	$ \pm\frac{1}{2}\rangle$
0.0	0.0	0	1	0
16.3(5)	16.5	0	0	1
70.0(5)	70.3	1	0	0

eigenvalues. Our refinement gives a ground-state doublet of pure  $|m_J = \pm\frac{3}{2}\rangle$  character. The threefold rotational symmetry at the rare-earth site implies that states within a time-reversal symmetry-paired Kramers doublet must be composed of  $m_J$  basis states separated by three units. Accordingly, in our case where the maximum  $m_J = \frac{5}{2}$ , it follows that the doublet composed of  $|m_J = \pm\frac{3}{2}\rangle$  cannot be coupled to any other basis state and is hence necessarily pure. The symmetry nature of this doublet imparts it with an exotic character: While two components of the pseudospin transform as a magnetic dipole, the third component transforms as a component of the magnetic octupole tensor [20]. Thus, the ground-state doublet in  $\text{Sm}_2\text{Ti}_2\text{O}_7$  is termed a dipolar-octupolar doublet. This result distinguishes  $\text{Sm}_2\text{Ti}_2\text{O}_7$  from other antiferromagnetic Kramers  $R_2\text{Ti}_2\text{O}_7$  pyrochlores ( $R = \text{Er}$  [21] and  $\text{Yb}$  [22]), which possess ground-state doublets that transform simply as a magnetic dipole, effectively mimicking a true  $S = \frac{1}{2}$ . Our refined  $g$ -tensor gives  $g_z = 0.857(9)$  and  $g_{xy} = 0.0$ , corresponding to Ising anisotropy, where the spins point along their local [111] direction, which connects the vertices of the tetrahedron to its center (inset of Fig. 1). The magnetic

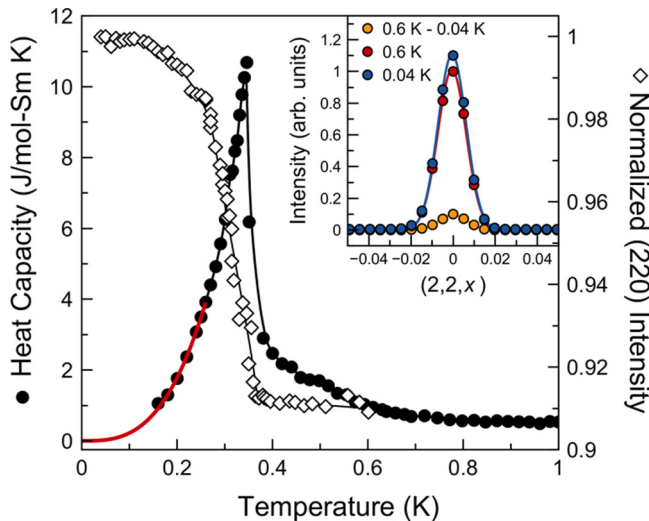


FIG. 2.  $\text{Sm}_2\text{Ti}_2\text{O}_7$  undergoes a long-range magnetic ordering transition at  $T_N = 0.35$  K. The black circles represent the heat capacity, which shows a sharp anomaly at  $T_N$  and a  $T^3$  dependence at the lowest temperatures, as indicated by the red line. The open diamonds represent the intensity of the (220) Bragg peak, which shows an abrupt increase at  $T_N$ . The black lines are guides to the eye. The inset shows a scan over the (220) Bragg peak above and below  $T_N$ , where the enhanced intensity corresponds to the formation of a magnetic Bragg peak.

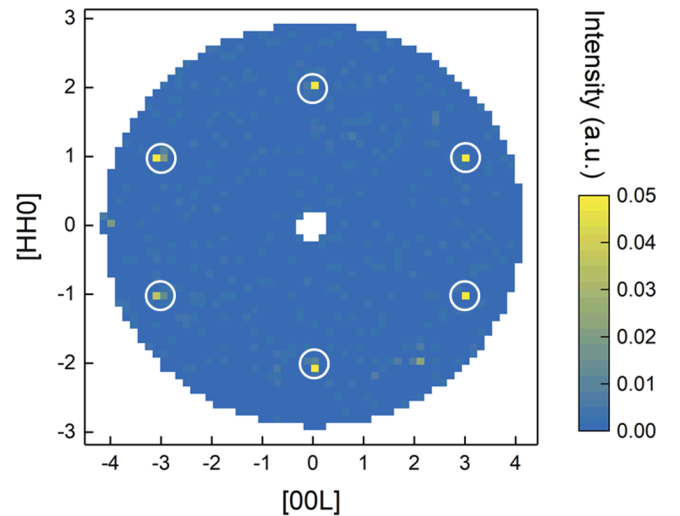


FIG. 3. Spin-flip channel of polarized neutron scattering measurements on  $\text{Sm}_2\text{Ti}_2\text{O}_7$  in the  $(HHL)$  scattering plane at 0.05 K. Magnetic Bragg peaks are observed to form on the (220) and (113) positions and are absent at the (111), (002), (222), and (004) positions. Symmetry analysis of this magnetic diffraction pattern reveals that  $\text{Sm}_2\text{Ti}_2\text{O}_7$  is ordering into the  $\Gamma_3$  AIAO state with an ordered moment of  $\mu_{\text{ord}} = 0.44(7)\mu_B$ . Note that weak bleed-through of nuclear Bragg intensity has been corrected by subtracting a high-temperature (4 K) data set.

moment within the ground-state doublet of  $\text{Sm}^{3+}$  is  $\mu_{\text{CEF}} = 0.43(6)\mu_B$ .

Finally, as originally discussed in Ref. [23], we can take advantage of the fact that extensive CEF studies have been performed on other rare-earth titanate pyrochlores [21,22,24–27], allowing us to use scaling arguments. An especially good starting point is  $\text{Er}^{3+}$  in  $\text{Er}_2\text{Ti}_2\text{O}_7$ , which has a large total angular momentum,  $J = 15/2$ . This material has seven excited crystal field levels, all of which were observed in a recent INS study, leading to a highly constrained CEF Hamiltonian [21]. Armed with these results, scaling arguments give us qualitatively good agreement with the known CEF manifolds for  $R_2\text{Ti}_2\text{O}_7$  ( $R = \text{Ho}$ ,  $\text{Tb}$ , and  $\text{Yb}$ ) [21]. When applied to  $\text{Sm}_2\text{Ti}_2\text{O}_7$ , these same scaling arguments predict the CEF ground state to be pure  $|m_J = \pm\frac{3}{2}\rangle$  with a large energy gap to the first excited state, consistent with our experimental determination.

We next turn to the low-temperature collective magnetic properties of  $\text{Sm}_2\text{Ti}_2\text{O}_7$ . The heat capacity of  $\text{Sm}_2\text{Ti}_2\text{O}_7$ , shown in Fig. 2(a), contains a lambda-like anomaly at  $T_N = 0.35$  K, indicative of a second-order phase transition to a long-range magnetically ordered state. This ordering transition was not observed in previous studies as their characterization measurements did not extend below 0.5 K [13]. The low-temperature region of the anomaly, below 0.3 K, is well fit by a  $T^3$  power law, consistent with gapless, three-dimensional antiferromagnetic spin waves. In order to compute the entropy release associated with this anomaly, we extrapolate the  $T^3$  behavior to 0 K. Then, an integration of  $C/T$  up to 1 K returns an entropy of  $0.84 R \ln 2$ , close to the full  $R \ln 2$  expected for a well-isolated Kramers doublet. Thus, a small fraction of the entropy release in this system may be taking place at

TABLE II. Bragg peak intensities for the possible  $\vec{k} = 0$  magnetic structures for  $\text{Sm}_2\text{Ti}_2\text{O}_7$ . The best agreement is obtained with the  $\Gamma_3$  all-in all-out structure.

	(111)	(002)	(222)	(220)	(113)	(004)
Observed	0	0	0	$1.0 \pm 0.4$	$0.78 \pm 0.27$	0
$\Gamma_3$	0	0	0	1.00	0.66	0
$\Gamma_5$	0.88	0	0	1	0.35	0
$\Gamma_7$	0.52	1.00	0.44	0.11	0	0
$\Gamma_9$ [110]	0.69	1.00	0.44	0.43	0.51	0.67
$\Gamma_9$ [100]	0.06	0.37	0.16	0.44	0.76	1.00

temperatures above 1 K or some fraction of the moment may remain dynamic below  $T_N$ .

We used the D7 polarized neutron scattering spectrometer at the ILL to search for magnetic diffuse scattering in  $\text{Sm}_2\text{Ti}_2\text{O}_7$ . While none could be resolved above or below  $T_N$ , we did observe the formation of magnetic Bragg peaks at the (220) and (113) positions in the spin-flip channel (Fig. 3). The observed magnetic Bragg reflections were indexed against the possible  $\vec{k} = 0$  ordered structures for the  $16c$  Wyckoff position in the  $Fd\bar{3}m$  pyrochlore lattice (Table II). The errors on the observed peak intensities are rather high due to the small magnetic signals ( $\mu_{\text{ord}} \leq \mu_{\text{CEF}} = 0.43\mu_B$ ) located on large nuclear Bragg peaks, the absorption from residual  $^{149}\text{Sm}$ , as well as the relatively poor  $Q$  resolution of a diffuse scattering instrument. However, as can be seen by careful examination of Table II, the observed magnetic Bragg reflections nicely map onto the  $\Gamma_3$  irreducible representation. All other representations can be ruled out by the absence of magnetic reflections at the (002) and (111) positions in the experimental data.  $\Gamma_3$  corresponds to the AIAO magnetic structure (right inset of Fig. 1), which is the expected result when Ising anisotropy is combined with net antiferromagnetic exchange interactions. The neutron order parameter, shown in Fig. 2, reveals a sharp onset below  $T_N = 0.35$  K, fully consistent with the anomaly observed in the heat capacity.

While the D7 data allowed a definitive determination of the magnetic structure of  $\text{Sm}_2\text{Ti}_2\text{O}_7$ , it is not appropriate for estimating the value of the ordered moment due to the coarse  $Q$  resolution of the instrument. The triple axis spectrometer HB-1A, with its significantly improved  $Q$  resolution, was therefore used for this purpose. Since HB-1A uses an unpolarized neutron beam, magnetic intensity was only observed at the (220) Bragg peak position in this experiment, which corresponds to the strongest magnetic reflection expected for the AIAO magnetic structure but also a relatively weak nuclear Bragg peak. We determined the  $\text{Sm}^{3+}$  ordered magnetic moment by comparing the ratio of the magnetic intensity to the nuclear intensity at this Bragg position. This procedure, which incorporated both the  $j_0$  and  $j_2$  spherical Bessel function contributions to the  $\text{Sm}^{3+}$  magnetic form factor, yielded an ordered moment of  $\mu_{\text{ord}} = 0.44(7)\mu_B$ .

Last, we turn to zero-field muon spin relaxation ( $\mu\text{SR}$ ) measurements on  $\text{Sm}_2\text{Ti}_2\text{O}_7$ , the results of which are presented in Fig. 4. The temperature-independent contribution from muons that land outside the sample has been subtracted, leaving only the sample asymmetry. At 1 K and above, the

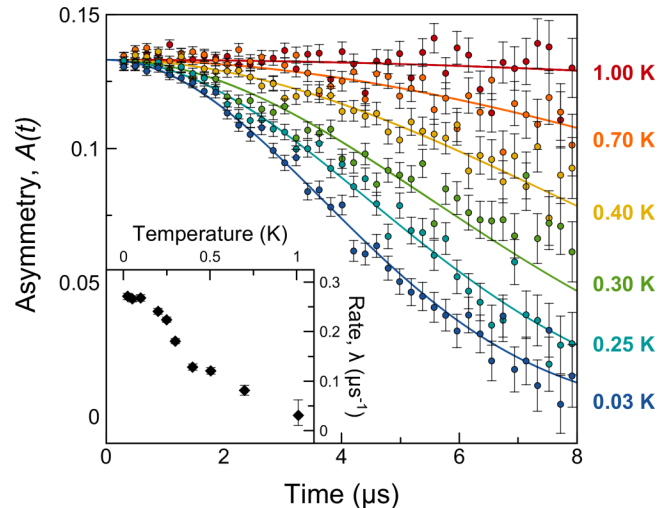


FIG. 4. The  $\mu\text{SR}$  asymmetry spectra of  $\text{Sm}_2\text{Ti}_2\text{O}_7$  between 1.00 and 0.03 K, which are well fit by a Gaussian relaxation, indicated by the solid lines. The temperature dependence of the relaxation rate  $\lambda$  extracted from these fits is shown in the inset. Below  $T_N$ ,  $\lambda$  is observed to plateau, indicative of persistent spin dynamics in the ordered state.

asymmetry is nonrelaxing, indicating that the  $\text{Sm}^{3+}$  moments are in a fast-fluctuating paramagnetic regime. Approaching  $T_N$ , the relaxation gradually increases, consistent with a critical slowing of the spin dynamics. Over the full temperature range, the asymmetry is well described by a Gaussian relaxation  $A(t) = A_0 e^{-\lambda t^2}$ , where  $\lambda$  is the temperature-dependent relaxation rate. The fitted relaxation rates, which are weak at all temperatures, are plotted in the inset of Fig. 4 where we see the rate sharply increase at  $T_N$  and then ultimately plateaus below 0.2 K.

In a small moment sample such as  $\text{Sm}_2\text{Ti}_2\text{O}_7$ , where the background relaxation is weak, one would expect to observe spontaneous oscillations in the asymmetry spectra below  $T_N$ . However, they are strikingly absent in our measurement. The Gaussian relaxation observed here, combined with the lack of oscillations in the asymmetry spectra below  $T_N$ , is reminiscent of recent  $\mu\text{SR}$  measurements on another Ising antiferromagnet,  $\text{Nd}_2\text{Zr}_2\text{O}_7$  [28]. In that case, the Gaussian relaxation was attributed to strong spin fluctuations that coexist microscopically with AIAO magnetic order, which generates a dynamic local magnetic field at the muon sites below  $T_N$ . This coexistence is argued to arise from magnetic moment fragmentation, which had been demonstrated in  $\text{Nd}_2\text{Zr}_2\text{O}_7$  via neutron scattering [8,10]. More specifically, the INS data on  $\text{Nd}_2\text{Zr}_2\text{O}_7$  revealed that the dynamic component of the ground state has a characteristic frequency on the order of  $10^{10}$  Hz which is well within the  $\mu\text{SR}$  timescale. The persistent spin dynamics observed in our  $\mu\text{SR}$  spectra for  $\text{Sm}_2\text{Ti}_2\text{O}_7$  could well arise from a similar origin. The absence of oscillations in an ordered state may also arise from a cancellation of the static dipolar field at the muon site from different ordered moments. However, this scenario is ruled out here by three simple observations: (1) There are no potential high-symmetry muon sites in the pyrochlore structure where the field could cancel by symmetry, (2) an oscillatory component *has been* observed

in the  $\mu$ SR of another AIAO pyrochlore  $\text{Nd}_2\text{Sn}_2\text{O}_7$  [6], where it is important to note that, unlike  $\text{Nd}_2\text{Zr}_2\text{O}_7$ , fragmentation physics has not been demonstrated, and (3)  $\text{Sm}_2\text{Ti}_2\text{O}_7$  is isostructural with  $\text{Nd}_2\text{Sn}_2\text{O}_7$  and therefore the muon stopping sites are expected to be very similar.

We have demonstrated that  $\text{Sm}_2\text{Ti}_2\text{O}_7$  possesses all the requisite ingredients for moment fragmentation physics. Crystal field analysis of our neutron spectroscopy measurements confirms that  $\text{Sm}_2\text{Ti}_2\text{O}_7$  has an Ising dipolar-octupolar crystal field ground-state doublet. Through symmetry analysis of our neutron diffraction data, we find that  $\text{Sm}_2\text{Ti}_2\text{O}_7$  orders into an all-in, all-out magnetic structure below  $T_N = 0.35$  K, with an ordered moment of  $\mu_{\text{ord}} = 0.44(7)\mu_B$ . Muon spin relaxation measurements identify persistent spin dynamics to temperatures well below  $T_N$  and an absence of oscillations.

This research was supported by NSERC of Canada. A portion of this research used resources at the High Flux Isotope Reactor and Spallation Neutron Source, a DOE Office of Science User Facility operated by the Oak Ridge National Laboratory. C.R.W. thanks the Canada Research Chair program (Tier II) and the CFI. C.M. thanks the Manitoba Government for support through the MGS. J.A.Q. acknowledges technical support from M. Lacerte and S. Fortier and funding from FRQNT and CFREF. G.S. thanks J. Lin and A. T. Savici for useful discussions, and support in the analysis. H.D.Z. acknowledges support from NSF DMR through Grant No. DMR-1350002. P.M.S. acknowledges financial support from the CCSF, the RSC and the University of Edinburgh through the GRS and PCDS.

- 
- [1] J. S. Gardner, M. J. P. Gingras, and J. E. Greedan, Magnetic pyrochlore oxides, *Rev. Mod. Phys.* **82**, 53 (2010).
- [2] M. J. Harris, S. T. Bramwell, D. F. McMorrow, T. Zeiske, and K. W. Godfrey, Geometrical Frustration in the Ferromagnetic Pyrochlore  $\text{Ho}_2\text{Ti}_2\text{O}_7$ , *Phys. Rev. Lett.* **79**, 2554 (1997).
- [3] A. P. Ramirez, A. Hayashi, R. J. Cava, R. Siddharthan, and B. S. Shastry, Zero-point entropy in spin ice, *Nature (London)* **399**, 333 (1999).
- [4] S. T. Bramwell and M. J. P. Gingras, Spin ice state in frustrated magnetic pyrochlore materials, *Science* **294**, 1495 (2001).
- [5] B. C. den Hertog and M. J. P. Gingras, Dipolar Interactions and Origin of Spin Ice in Ising Pyrochlore Magnets, *Phys. Rev. Lett.* **84**, 3430 (2000).
- [6] A. Bertin, P. D. de Réotier, B. Fåk, C. Marin, A. Yaouanc, A. Forget, D. Sheptyakov, B. Frick, C. Ritter, A. Amato *et al.*,  $\text{Nd}_2\text{Sn}_2\text{O}_7$ : An all-in–all-out pyrochlore magnet with no divergence-free field and anomalously slow paramagnetic spin dynamics, *Phys. Rev. B* **92**, 144423 (2015).
- [7] J. Xu, V. K. Anand, A. K. Bera, M. Frontzek, D. L. Abernathy, N. Casati, K. Siemensmeyer, and B. Lake, Magnetic structure and crystal-field states of the pyrochlore antiferromagnet  $\text{Nd}_2\text{Zr}_2\text{O}_7$ , *Phys. Rev. B* **92**, 224430 (2015).
- [8] E. Lhotel, S. Petit, S. Guitteny, O. Florea, M. C. Hatnean, C. Colin, E. Ressouche, M. R. Lees, and G. Balakrishnan, Fluctuations and All-in–All-Out Ordering in Dipole-Octupole  $\text{Nd}_2\text{Zr}_2\text{O}_7$ , *Phys. Rev. Lett.* **115**, 197202 (2015).
- [9] V. K. Anand, A. K. Bera, J. Xu, T. Herrmannsdörfer, C. Ritter, and B. Lake, Observation of long-range magnetic ordering in pyrochlore  $\text{Nd}_2\text{Hf}_2\text{O}_7$ : A neutron diffraction study, *Phys. Rev. B* **92**, 184418 (2015).
- [10] S. Petit, E. Lhotel, B. Canals, M. C. Hatnean, J. Ollivier, H. Mutka, E. Ressouche, A. R. Wildes, M. R. Lees, and G. Balakrishnan, Observation of magnetic fragmentation in spin ice, *Nat. Phys.* **12**, 746 (2016).
- [11] M. E. Brooks-Bartlett, S. T. Banks, L. D. C. Jaubert, A. Harman-Clarke, and P. C. W. Holdsworth, Magnetic-Moment Fragmentation and Monopole Crystallization, *Phys. Rev. X* **4**, 011007 (2014).
- [12] O. Benton, Quantum origins of moment fragmentation in  $\text{Nd}_2\text{Zr}_2\text{O}_7$ , *Phys. Rev. B* **94**, 104430 (2016).
- [13] S. Singh, S. Saha, S. K. Dhar, R. Suryanarayanan, A. K. Sood, and A. Revcolevschi, Manifestation of geometric frustration on magnetic and thermodynamic properties of the pyrochlores  $\text{Sm}_2\text{X}_2\text{O}_7$  ( $X = \text{Ti}, \text{Zr}$ ), *Phys. Rev. B* **77**, 054408 (2008).
- [14] D. L. Abernathy, M. B. Stone, M. J. Loguillo, M. S. Lucas, O. Delaire, X. Tang, J. Y. Y. Lin, and B. Fultz, Design and operation of the wide angular-range chopper spectrometer ARCS at the Spallation Neutron Source, *Rev. Sci. Instrum.* **83**, 015114 (2012).
- [15] G. E. Granroth, A. I. Kolesnikov, T. E. Sherline, J. P. Clancy, K. A. Ross, J. P. C. Ruff, B. D. Gaulin, and S. E. Nagler, SEQUOIA: A newly operating chopper spectrometer at the SNS, *J. Phys.: Conf. Ser.* **251**, 012058 (2010).
- [16] See Supplemental Material at <http://link.aps.org/supplemental/10.1103/PhysRevB.98.100401> for further information on the crystal growth, experimental details, and the crystal field analysis, which includes Refs. [18,21,23,29–35].
- [17] B. Z. Malkin, T. T. A. Lummen, P. H. M. Van Loosdrecht, G. Dhalle, and A. R. Zakirov, Static magnetic susceptibility, crystal field and exchange interactions in rare earth titanate pyrochlores, *J. Phys.: Condens. Matter* **22**, 276003 (2010).
- [18] J. Y. Y. Lin, H. L. Smith, G. E. Granroth, D. L. Abernathy, M. D. Lumsden, B. Winn, A. A. Aczel, M. Aivazis, and B. Fultz, MCViNE—an object oriented Monte Carlo neutron ray tracing simulation package, *Nucl. Instrum. Methods Phys. Res.* **810**, 86 (2016).
- [19] M. Blume, A. J. Freeman, and R. E. Watson, Theory of spin-orbit coupling in atoms. III, *Phys. Rev.* **134**, A320 (1964).
- [20] Y.-P. Huang, G. Chen, and M. Hermele, Quantum Spin Ices and Topological Phases from Dipolar-Octupolar Doublets on the Pyrochlore Lattice, *Phys. Rev. Lett.* **112**, 167203 (2014).
- [21] J. Gaudet, A. M. Hallas, A. I. Kolesnikov, and B. D. Gaulin, Effect of chemical pressure on the crystal electric field states of erbium pyrochlore magnets, *Phys. Rev. B* **97**, 024415 (2018).
- [22] J. Gaudet, D. D. Maharaj, G. Sala, E. Kermarrec, K. A. Ross, H. A. Dabkowska, A. I. Kolesnikov, G. E. Granroth, and B. D. Gaulin, Neutron spectroscopic study of crystalline electric field excitations in stoichiometric and lightly stuffed  $\text{Yb}_2\text{Ti}_2\text{O}_7$ , *Phys. Rev. B* **92**, 134420 (2015).
- [23] M. T. Hutchings, Point-charge calculations of energy levels of magnetic ions in crystalline electric fields, in *Solid State Physics*, edited by F. Seitz and D. Turnbull (Academic, New York, 1964), Vol. 16, pp. 227–273.

- [24] S. Rosenkranz, A. P. Ramirez, A. Hayashi, R. J. Cava, R. Siddharthan, and B. S. Shastry, Crystal-field interaction in the pyrochlore magnet  $\text{Ho}_2\text{Ti}_2\text{O}_7$ , *J. Appl. Phys.* **87**, 5914 (2000).
- [25] A. Bertin, Y. Chapuis, P. D. de Réotier, and A. Yaouanc, Crystal electric field in the  $R_2\text{Ti}_2\text{O}_7$  pyrochlore compounds, *J. Phys.: Condens. Matter* **24**, 256003 (2012).
- [26] M. Ruminy, E. Pomjakushina, K. Iida, K. Kamazawa, D. T. Adroja, U. Stuhr, and T. Fennell, Crystal-field parameters of the rare-earth pyrochlores  $R_2\text{Ti}_2\text{O}_7$  ( $R = \text{Tb}, \text{Dy}, \text{and Ho}$ ), *Phys. Rev. B* **94**, 024430 (2016).
- [27] A. J. Princep, H. C. Walker, D. T. Adroja, D. Prabhakaran, and A. T. Boothroyd, Crystal field states of  $\text{Tb}^{3+}$  in the pyrochlore spin liquid  $\text{Tb}_2\text{Ti}_2\text{O}_7$  from neutron spectroscopy, *Phys. Rev. B* **91**, 224430 (2015).
- [28] J. Xu, C. Balz, C. Baines, H. Luetkens, and B. Lake, Spin dynamics of the ordered dipolar-octupolar pseudospin-1/2 pyrochlore  $\text{Nd}_2\text{Zr}_2\text{O}_7$  probed by muon spin relaxation, *Phys. Rev. B* **94**, 064425 (2016).
- [29] A. S. Wills, A new protocol for the determination of magnetic structures using simulated annealing and representational analysis (SARAh), *Physica B* **276**, 680 (2000).
- [30] J. Rodríguez-Carvajal, Recent advances in magnetic structure determination by neutron powder diffraction, *Physica B* **192**, 55 (1993).
- [31] M. Ruminy, M. N. Valdez, B. Wehinger, A. Bosak, D. T. Adroja, U. Stuhr, K. Iida, K. Kamazawa, E. Pomjakushina, D. Prabhakaran *et al.*, First-principles calculation and experimental investigation of lattice dynamics in the rare-earth pyrochlores  $R_2\text{Ti}_2\text{O}_7$  ( $R = \text{Tb}, \text{Dy}, \text{Ho}$ ), *Phys. Rev. B* **93**, 214308 (2016).
- [32] K. W. H. Stevens, Matrix elements and operator equivalents connected with the magnetic properties of rare earth ions, *Proc. Phys. Soc., London, Sect. A* **65**, 209 (1952).
- [33] U. Walter, Treating crystal field parameters in lower than cubic symmetries, *J. Phys. Chem. Solids* **45**, 401 (1984).
- [34] J. L. Prather, *Atomic Energy Levels in Crystals*, NBS Monograph No. 19 (National Bureau of Standards, Gaithersburg, MD, 1961).
- [35] O. Knop, F. Brisse, and L. Castelliz, Pyrochlores V: Thermoanalytic, x-ray, neutron, infrared, and dielectric studies of  $A_2\text{Ti}_2\text{O}_7$  titanates, *Can. J. Chem.* **47**, 971 (1969).